New Zealand Journal of Marine and Freshwater Research, 2006, Vol. 40: 305–324
0028–8330/06/4002–0305

Tidal circulation in Tasman and Golden Bays: implications for river plume behaviour

BENJAMIN J. TUCKEY
MARK T. GIBBS
BENJAMIN R. KNIGHT
PAUL A. GILLESPIE
Cawthron Institute
Private Bag 2
Nelson
New Zealand
email: mark.gibbs@cawthron.org.nz

Abstract An investigation into the tidal residual circulation in the Tasman/Golden Bays system was performed. This investigation involved collecting hydrographic and current meter data, and configuring a numerical circulation model. The model was able to reproduce the gross features of the major tidal flows within the system revealed by the data. The simulated tidal residual circulation conformed to that previously suggested, except along the western side of Tasman Bay where this investigation suggests that residual flows move northwards. The validated model was then used to produce simulations of the fate of the plumes from the major rivers. Salinity field simulations describing different river flow and wind direction/velocity scenarios suggest that the Motueka River plume can cover considerable proportions of western side Tasman Bay, extending into Golden Bay during flood conditions. The embedded sediment transport model was also used to investigate the fate of fine sediments entering the bays. Simulated distribution patterns of fine sediments entering the bays from the four major tributaries were found to be consistent with existing bathymetric and seabed substrate characteristics.

Keywords Tasman Bay; tidal circulation; tidal model; New Zealand

M04117; Online publication date 3 May 2006
Received 2 June 2004; accepted 12 June 2005

INTRODUCTION

Tasman Bay and Golden Bay, often referred to as the Nelson Bays, are positioned next to each other near the northwest corner of the South Island (Fig. 1). Both bays are wide, shallow inlets and open out to Cook Strait, which separates New Zealand's two main landmasses. The Nelson Bays represent a significant economic and cultural resource for the region. For example, the bays support regionally important scallop and finfish fisheries, and are used extensively for recreational fishing and boating and supply spat for the commercial shellfish farming industry (J. Wilson, Sealord Shellfish Ltd, Nelson pers. comm.). The bays also play a strong role for indigenous Maori communities and have high cultural values. The bays also perform important goods and services roles including assimilating waste products from both urban and rural communities in the region. Furthermore, the New Zealand coastline does not feature many extensive coastal inlets, and hence the Nelson Bays region is important nationally.

The Nelson region has supported the fastest population growth in New Zealand for a number of years and hence the bays are exposed to increasing anthropogenic activities; e.g., recreational fishing, wastewater disposal, urban shoreline development. There is therefore a real demand for increased understanding about the structure and functioning of the bays and the aim of the work presented here is to understand and simulate the dominant hydrodynamical processes occurring within the bays.

As noted by Baker (1972) and Heath (1969, 1976), most of the variability in circulation within the bays is associated with tidal flows. However, tidal flows in the adjoining Cook Strait are complex, as New Zealand is centred on a degenerate antiamphidrome (Goring & Walters 2002). The M_2 semidiurnal tide, with a period of 12.42 h, forms a resonant trapped wave that rotates counter clockwise around New Zealand (Bye & Heath 1975; Proctor & Hadfield 1998; Stanton et al. 2001; Walters et al. 2001; Goring & Walters 2002). This trapped wave creates

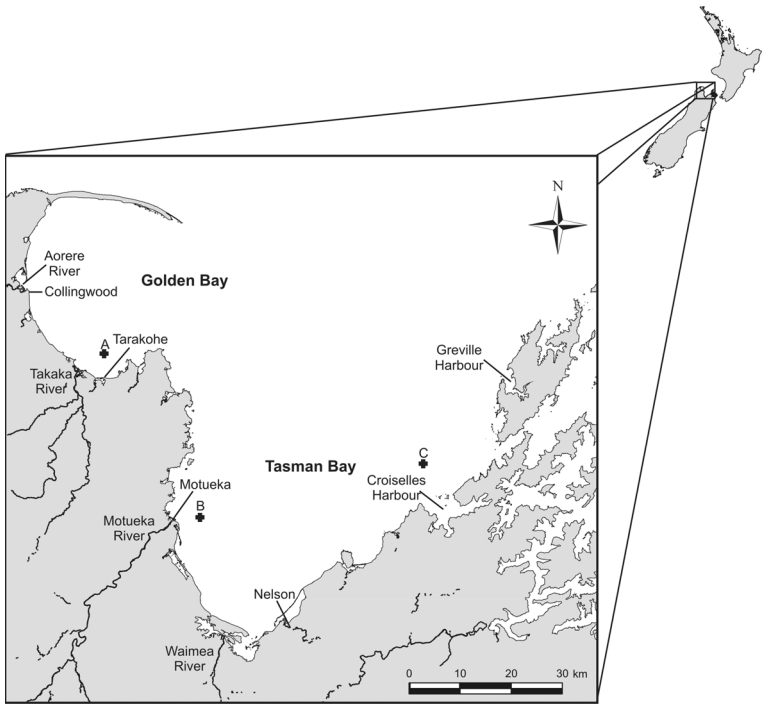

Fig. 1 Location map showing Tasman and Golden Bays at the northern end of the South Island of New Zealand and major river inflows. The bays open out to Cook Strait that separates New Zealand's North Island from the South Island. Current meter deployment sites are marked by crosses (A, B, and C).

a difference in phase as large as 140° across the eastern and western boundaries of the Cook Strait and results in strong flows and interactions between tidal processes within the central region of New Zealand (Heath 1977).

Heath (1976) reviewed the results of several drift card releases, direct current measurements taken over less than 2 days and a crude numerical model, and suggested the following features of the circulation within the bays: (1) current flows are primarily associated with tidal flows; (2) local wind-driven flows can act to alter the tidal flows; and (3) the residual circulation flows in a clockwise direction in Golden Bay, and in an anti-clockwise direction in Tasman Bay.

This last feature is represented in Fig. 2, extracted from Heath (1976). This figure shows the suggested residual circulation in the bays. The Heath (1976) model suggested that the clockwise residual circulation in Golden Bay, along with the mean easterly flow north of Farewell Spit acts to transport sediment in a way that extends the Spit, and this is consistent with geological evidence of sediment transport (Van Der Linden 1969). It is also thought that coarse sediments exiting from the Motueka River are transported to the east, however this is likely to be more to do with littoral drift associated with wind waves than residual tidal transport. However, recent evidence (MacKenzie 2004) suggests that the Moteuka plume commonly gets transported to the north, the opposite direction to the residual flow suggested by Heath (1976). Therefore Heath's (1976) suggested general counterclockwise residual circulation in Tasman Bay may not be quite correct on the western side of Tasman Bay, and this is investigated in detail here.

The work presented here seeks to satisfy the following objectives. To: (1) develop a numerical model capable of simulating the hydrodynamic flows within Tasman and Golden Bays; (2) understand the tidal circulation in Tasman and Golden Bays; and (3) investigate the behaviour of the Motueka River plume in terms of salinity and suspended sediments.

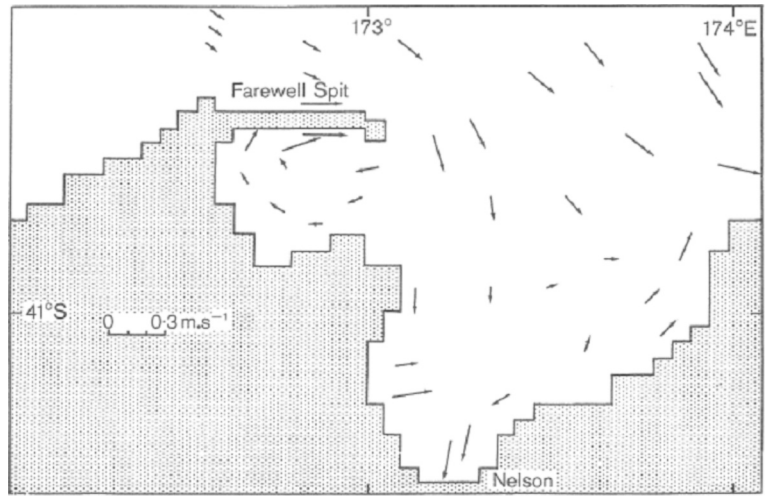

Fig. 2 Residual circulation figure reproduced from Heath (1976).

METHODS

Current data were collected from three locations (Fig. 1) within the Tasman/Golden Bay system. Two fixed current meters were deployed for 30-day periods at a Golden Bay site (A), starting at 1000 h on 18 July 2002 (approximately low tide, Nelson). The current meters were positioned on the same mooring with one instrument located 3 m and the other 13 m above the sea floor. The total water depth at the site was 15 m. An Acoustic Doppler Profiler (ADP) was deployed in western Tasman Bay (site B in Fig. 1) for a 33-day period starting at 0922 h on 6 July 2002. A fixed current meter was also deployed in eastern Tasman Bay (site C) for a 22-day period starting at 1036 h on 26 April 2001. This current meter was located at a depth of 20 m, approximately in the middle of the water column.

The numerical tidal harmonic package of Foreman (1977) was then used to calculate the amplitude and Greenwich phase of the harmonic tidal constituents for each of seven ports (Collingwood, Tarakohe, Motueka, Nelson, Croiselles Harbour, Greville Harbour, Stephens Island) within the Tasman/Golden Bays system. Data of tide heights were created by interpolating tide height information contained in the New Zealand Nautical Almanac (2002).

To investigate the fate and behaviour of the plume for the Motueka River, observations of the Motueka plume behaviour were obtained by performing conductivity-temperature-depth (CTD) surveys. Two surveys encompassing the western side of Tasman Bay were performed; one during a period of low flow (7–8 March 2001) and the other during a period of high flow (9–10 May).

The Environmental Fluid Dynamics Computer Code (EFDC, Hamrick 1992) was applied to the Tasman/Golden Bays system. EFDC is based on the numerical schemes from the Princeton Ocean Model (Blumberg & Mellor 1987) and is well suited to these types of coastal ocean applications (Gibbs et al. 1998; Marchesiello & Middleton 2000). EFDC features sigma coordinates in the vertical and Cartesian or curvilinear, orthogonal horizontal coordinates. The model solves the three-dimensional, vertically hydrostatic, free surface, turbulent averaged equations for a fluid of variable density. It also solves dynamically coupled transport equations for turbulent kinetic energy, turbulent length scale, salinity, and temperature.

EFDC incorporates mode-splitting (Simons 1974; Madala & Piaseck 1977) to separate the vertically integrated equations (external free surface gravity wave or barotropic mode) from the vertical structure equations (internal shear or baroclinic mode) and permits the calculation of the free surface elevation, by solving the velocity transport separately from the three-dimensional calculation of the velocity and the thermodynamic properties. The external mode equations are obtained by integrating the internal mode equations over the depth, consequently

removing all vertical structure (Mellor 1998). The equation for surface elevation is therefore:

$$\frac{\partial \eta}{\partial t} + \frac{\partial \bar{u} D}{\partial x} + \frac{\partial \bar{v} D}{\partial y} = 0 \quad (1)$$

the momentum equations are as follows:

$$\frac{\partial \bar{u} D}{\partial t} + \frac{\partial \bar{u}^2 D}{\partial x} + \frac{\partial \bar{u}\bar{v} D}{\partial y} - \bar{F}_x - f\bar{v}D + gD\frac{\partial \eta}{\partial x} = \frac{\tau_x}{\rho_W} - C_D u\sqrt{u^2 + v^2} \quad (2)$$

$$\frac{\partial \bar{v} D}{\partial t} + \frac{\partial \bar{u}\bar{v} D}{\partial x} + \frac{\partial \bar{v}^2 D}{\partial y} - \bar{F}_y - f\bar{u}D + gD\frac{\partial \eta}{\partial x} = \frac{\tau_y}{\rho_W} - C_D v\sqrt{u^2 + v^2} \quad (3)$$

where

$$\bar{u} \equiv \int_{-1}^{0} u\partial\sigma \text{ and } \bar{v} \equiv \int_{-1}^{0} v\partial\sigma \quad (4)$$

are the depth averaged velocities in the x and y directions respectively and t represents time. η is the surface elevation, while $D = H + \eta$ is the instantaneous water depth where H is the depth below the mean sea level, ρ_w is the density of sea water, and f is the Coriolis coefficient. F_x and F_y are the horizontal diffusion terms. τ_x and τ_y are the wind stress components in the x and y direction. The x direction increases when moving east and the y direction increases when moving north. C_D is the bottom friction assuming a constant drag law and a logarithmic boundary layer:

$$C_D = \left(\frac{1}{\kappa}\ln\frac{z}{z_o}\right)^{-2} \quad (5)$$

where κ is the von Kármán's constant, z_o is the roughness length, and z is dependent on the depth and the distance between the bottom and the adjacent following vertical layer. The above equations assume that water is incompressible and that any hydrostatic and density variations are insignificant.

The initial values of η, u, and v are zero within the model domain while the open boundaries are determined by:

$$\eta = \eta_0 \sin \omega t \quad (6)$$

where η_0, is the amplitude of the tidal constituents and ω is the frequency of the tidal constituents. The four major constituents were used to force the model. For the closed boundaries of the model domain, EFDC uses a half-slip boundary condition where only the velocities that are normal to the boundary go to zero and non-normal velocities are reflected back into the domain without loss of energy.

A number of grids of different resolution were configured. Initially a resolution of 200 m was used, however the results using lower resolution grids were almost identical, hence the results presented here are from an orthogonal grid using control volume dimensions of 2500 m by 2500 m. Five layers in the vertical were used and the domain extended into Cook Strait so that the boundary was a considerable distance from the region under consideration. The bathymetry data for both bays were obtained from Royal New Zealand Navy Hydrographic Chart No. 61, adjusted to mean sea level and were interpolated linearly into the model grid. Also included in the Tasman/Golden Bays model were fresh water inputs, i.e., rivers. The four rivers that were deemed significant enough to include in the model, Waimea, Motueka, Takaka, and Aorere, are displayed in Fig. 1.

The model was forced by prescribing surface elevation boundary conditions at the open-ocean boundary and this proved to be particularly problematic. Two approaches were taken to determine these conditions. The first was to use the results from the Bowman et al. (1980) Cook Strait model, the second was to configure EFDC for Cook Strait. The Bowman et al. (1980) model was a barotropic model and although reasonable agreement between sea-level measurements around Cook Strait were obtained by these investigators, configuring the three-dimensional Bays model using boundary conditions from the Bowman Cook Strait model did not result in adequate agreement with sea-level measurements within the bays. As a result, EFDC was configured for Cook Strait using known open ocean boundary conditions at either end of Cook Strait. This low-resolution model was then run to provide a sea-level elevation boundary condition for the high-resolution Bays model. This boundary condition was a linear combination of the four major tidal constituents, the phase of each of which varied across the boundary. An open ocean boundary corresponding to French Pass also had to be included in the model. This boundary is very important as French Pass is a very deep narrow channel of water and therefore generates high velocity currents (mean

cross-channel currents measured as high as 60 cm/s although instantaneous currents can be significantly greater). These high discharges have an effect on the tidal circulation within Tasman Bay. The amplitude and phase for this boundary was determined using differences in the phase and amplitude of sea-level data from French Pass and Stephens Island.

The Motueka River plume was investigated numerically under a range of conditions for estimated baseline and flood flow situations. Simulations were performed with a constant flow rate of 50 $m^3 s^{-1}$ (moderate rainfall event), 200 $m^3 s^{-1}$ (significant flood event), and 1000 $m^3 s^{-1}$ (large flood event) for the Motueka River over a period of 10 days. Simulations were performed with no wind forcing and 20 knot winds in the direction of the prevailing winds for Tasman Bay; northerlies, north easterlies, and south westerlies.

EFDC contains a sediment transport sub-model and this was used (with the same grid resolution) to investigate the fate of suspended sediments delivered to the Nelson Bays from the four major rivers, the Aorere, Takaka, Motueka, and Waimea (Fig. 1), which deliver the majority of sediment to Tasman and Golden Bay (Harris 1990). Amongst these rivers, the Motueka drains the largest catchment area and contributes the highest annual suspended sediment (SS) load (Table 1). The transport of cohesive sediments of three grain sizes delivered into the bays from the four major rivers were modelled. For the 2 μm (clay), 10 μm (fine silt), and 20 μm (very fine silt) grain size fractions, the corresponding settling velocities assigned were 10^{-5} m s^{-1}, 10^{-4} m s^{-1}, and 3×10^{-4} m s^{-1}, respectively (Hamerick 2001). Simulations were performed under different wind conditions; i.e., no wind and 10 or 15 knot northerlies. The sediment concentration for each of the modelled size classes was assumed to be 5% of the total SS concentration shown in Table 1. This value was assigned based on particle size distributions for SS from various rivers around the world (Carlow & Petts 1992). Coarser grain sediments were also modelled but, as the spatial impact from these was restricted to short distances

Table 1 Mean flow and sediment load for the largest rivers discharging into Tasman and Golden Bay, New Zealand.

River	Catchment area[1] (km^2)	Discharge[1] ($m^3 s^{-1}$)	Sediment load[2] (Mt)
Waimea	726	20	0.11[3]
Motueka	2019	68	0.35
Takaka	890	60	0.07
Aorere	702	84	012

[1]Data from M. Doyle, Tasman District Council.
[2]Data from Basher & Hicks (2003) and M. Hicks (NIWA, Christchurch pers. comm.).
[3]Probably an overestimate (L. Basher, Landcare, Nelson pers. comm.).

Table 2 Baseline and flood flow and the total suspended sediment (SS) load concentration for major tributaries of the Nelson Bays, New Zealand.

	Flow ($m^3 s^{-1}$)		Total SS load (mg $litre^{-1}$) [2]	
River	Baseline	Flood event[1]	Baseline	Flood event
Waimea	9	280	5	500
Motueka	40	480	5	500
Takaka	35	475	5	300
Aorere	36	850	5	250

[1] Average over a 10-day period encompassing the event.
[2] Assigned approximate values based on Basher & Hicks (2003), Gillespie et al. (2001), Nottage (2001), R. Young (Cawthron Institute, Nelson pers. comm.) and M. Hicks (NIWA, Christchurch pers. comm.).

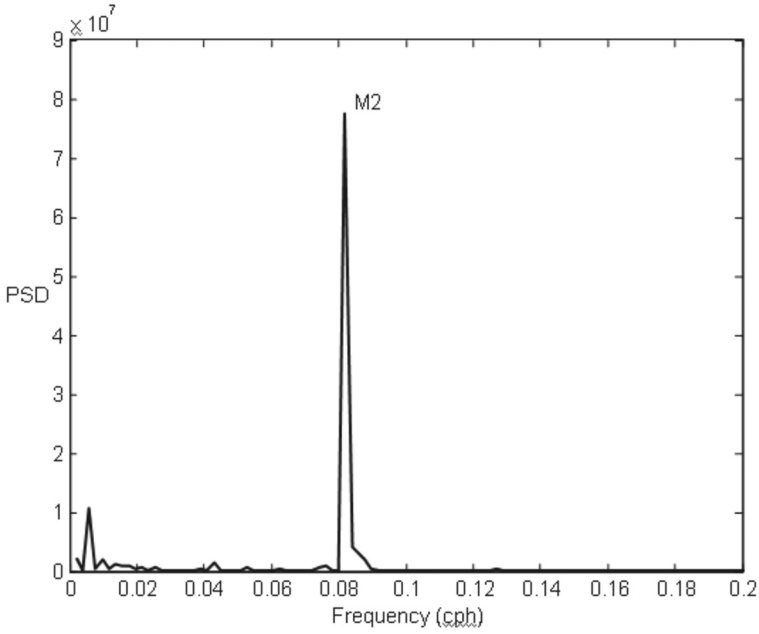

Fig. 3 Spectral analysis of northern component of velocity data collected close to Motueka River mouth, New Zealand.

Table 3 Greenwich phases and amplitudes from harmonic analysis of tidal data, and M_2 phases and amplitudes from Bowman et al. (1980) for Wellington (amplitude in metres and phase in degrees) for major ports within the Tasman/Golden Bay System, New Zealand.

	Collingwood	Tarakohe	Motueka	Nelson	Croiselles Harbour	Greville Harbour	Stephens Island
M_2							
Amplitude	1.66	1.37	1.26	1.37	1.56	1.18	0.86
Phase	71.28	51.53	79.16	83.41	76.12	73.76	69.04
S_2							
Amplitude	0.33	0.30	0.39	0.37	0.32	0.27	0.22
Phase	137.14	116.00	143.98	153.77	141.98	138.78	132.91
N_2							
Amplitude	0.36	0.29	0.21	0.29	0.32	0.29	0.16
Phase	41.56	21.95	47.87	53.17	46.18	44.03	38.05

from the plume, only fine grain sediments were used for this analysis.

Two river flow scenarios were applied: a baseline flow and a significant flood flow for each river. The base flow was estimated from long-term flow records and flood flow is an averaged flow (not to be confused with the peak flow) over the 10-day period encompassing the storm event. Baseline and flood flow rates for each river and representative total SS concentrations were assigned after reviewing the available data for the rivers concerned (Table 2).

Non-cohesive sediment transport (i.e., fine sand) was not modelled as the transport of non-cohesive sediments is largely influenced by combined wave and current action, and waves are not accounted for in the hydrodynamic model. Furthermore, Gibbs (2001) highlighted that there is considerable resuspension of sediments within the bays. The EFDC model allows for resuspension of cohesive sediment by specifying a resuspension rate that is calculated when the stress on the sediment exceeds a critical level.

RESULTS AND DISCUSSION

Tidal circulation

The power spectral density (PSD) of the depth averaged currents from site B in western Tasman Bay is shown in Fig. 3. The results from the spectral analysis of these data (and all current data) indicate that the semi-diurnal, particularly M_2, component was dominant. The frequency resolution of these data was such that influences from other tidal constituents would be indicated by a separate spectral peak from the peak identified as the M_2 tide. The identified spike has a frequency of 0.0805 cycles per h (cph) which equates to an approximate period of 12.42 h, the period of the M_2 tide.

The amplitude and phase of the three major constituents determined from the 2-year harmonic analysis of the tidal data are shown in Table 3. A comparison of the amplitudes of the three tidal constituents at seven Nelson Bays ports (Table 3) shows that, on average, the M_2 tidal constituent was greater than the S_2 tidal constituent by a factor of c. 4 and greater than the N_2 tidal constituent by a factor of c. 5. This was consistent with the results from the spectral analysis.

Inspection of the tidal phases (from the locations shown in Fig. 1) provided information on how the tide, generally propagating as a Kelvin wave, propagates around the region. It is of interest that the phases and amplitudes at the locations within the bays system fail to show a consistent trend. Heath (1976) suggested that this was owing to the following factors. First, the tidal processes within the bays are the net effect of contributions from both a Kelvin wave propagating within Cook Strait, but also from the Kelvin wave propagating southwards along the west coasts of both islands. Second, some of the tidal stations are located within large shallow estuaries and bottom friction within these estuaries can act to alter the local tidal response. Therefore, in summary, the tidal circulation within the bays is not straightforward and is the net effect of multiple input signals even for the dominant M_2 constituent.

Inspection of the depth-averaged current data acquired during the deployments (Fig. 4) revealed the dominance of the semi-diurnal tidal signal at all three sites where current meters were deployed. The mean current speeds, tidally averaged, were 0.54 cm s^{-1} at site A, 2.35 cm s^{-1} at site B, and 2.13 cm s^{-1} at site C.

Fig. 4 shows comparisons between the observed and simulated depth-averaged currents. Each plot in Fig. 4 has been aligned so that the data and

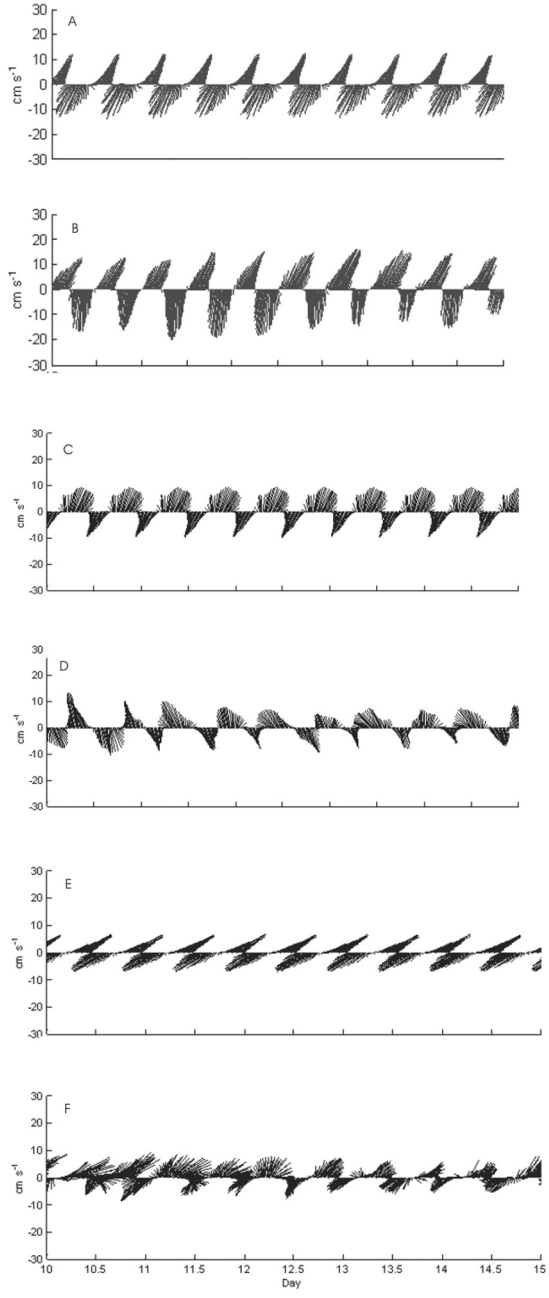

Fig. 4 Simulated and observed depth-averaged currents from: **A**, **B**, eastern Tasman Bay; **C**, **D**, western Tasman Bay; **E**, **F**, eastern Golden Bay.

simulated currents start at the same stage of the tide. Inspection of these plots revealed that the general behaviour and phase of the simulated currents were in reasonable agreement with the observations. This result is pleasing given the complexity of the bathymetry and tidal forcing in the region. For the site in eastern Tasman Bay (Fig. 4), the magnitude of the simulated currents was higher than the observed (maximum simulated ebb tide current speed ≈ 18 cm s^{-1} compared with maximum observed ebb tide current speed ≈ 12 cm s^{-1} and maximum simulated flood tide current speed ≈ 20 cm s^{-1} compared with maximum observed flood tide current speed ≈ 16 cm s^{-1}). The observed and predicted directions for the ebb tide and flood tide were similar. The flood tidal flows are primarily directed southwards along the western coast of D'Urville Island and the ebb flows were directed slightly more to the east as a result of French Pass.

For the western Tasman Bay site (Fig. 4), the magnitude of the simulated currents compared well to the observed currents (maximum current speed ≈ 10 cm s^{-1}), however the difference between the principal axes of the simulated and observed depth-averaged currents was 16°. Fig. 4 shows the simulated and observed currents from the Golden Bay site. This figure shows that there was good agreement between the flow directions, and magnitudes of the flows (maximum current speed ≈ 5 cm s^{-1}). The non-tidal northerly flows at the start of the record coincided with persistent southerly winds.

The performance of the model was investigated by comparing the simulated and observed amplitudes and phases of the sea level. A harmonic analysis was performed at positions within the model domain corresponding to seven ports (Table 3). Table 4 presents the comparison between relative phases and amplitudes of the M_2 tide. Considering first the eastern side of Tasman Bay (Stephens Island to Nelson), both the observations and model suggest that the tide propagated to the South and the time of high tide lagged towards Nelson (decreasing phase). The observed and simulated relative amplitude also decreased into the bay along this side. Similarly, the trend in the phases of the simulated sea-level perturbations was in good agreement with the observations although the model predicted a smaller discrepancy for Tarakohe. The model also under-predicted the amplitude at Collingwood. However, despite these differences the dominant trends of the phases and amplitudes were simulated by the model.

The phase difference between sea surface elevations and currents gives insight into the dynamics of the tidal processes and the model performance. If the elevation and currents are in phase, then the tide is propagating as a progressive wave. By contrast, a phase difference of 90° suggests a standing wave. For sites A, B, and C, the phase difference between the observed and simulated currents was calculated relative to high tide at the closest port. At site A the phase difference of the observed currents was 80°, whereas the phase difference of the simulated currents was also 80°. At site B the phase difference of the observed currents was 94°, whereas the phase difference of the simulated currents was 80°. At site C the phase difference of the observed currents was 94°, whereas the phase difference of the simulated currents was 101°. The simulated and observed phase differences compared well for all sites and suggest that a standing wave exists within Tasman and Golden Bay. This is consistent with high tide at Nelson lagging the rest of the bays, which would be inconsistent with a progressive wave travelling around Tasman and Golden Bay.

Table 4 Relative phases and amplitudes of M_2 tide, relative to Nelson, New Zealand, from harmonic analysis of predicted tidal and model data (amplitude in metres and phase in degrees) for major ports within the Tasman/Golden Bay System.

Port	Observed relative phase	Observed relative amplitude	Simulated relative phase	Simulated relative amplitude
Collingwood	–12.13	0.30	–4.90	0.02
Tarakohe	–31.88	0.01	–6.25	–0.01
Motueka	–4.25	–0.10	–5.79	–0.01
Nelson	0.00	0.00	0.00	0.00
Croiselles Harbour	–7.29	0.19	–11.05	–0.09
Greville Harbour	–9.65	–0.19	–12.09	–0.18
Stephens Island	–14.37	–0.50	–14.02	–0.35

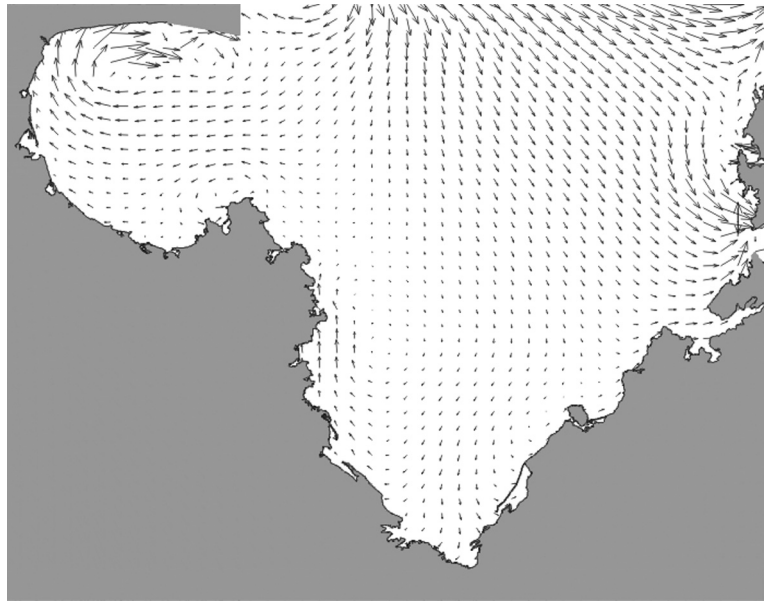

Fig. 5 Simulated depth-averaged tidal residual circulation for Tasman Bay/Golden Bay, New Zealand. The largest currents (20 cm s^{-1}) occur over the shallow banks inside Farewell Spit (top left).

The tidal residual, or tidally-averaged circulation is mostly associated with differences in the spatial pattern of the rising tide and the falling tide. Comparison between the tidal residual circulation predicted by the Tasman Bay/Golden Bay model (Fig. 5) and the Heath (1976) prediction (Fig. 2) showed that the two are very similar. Both predicted a mean clockwise circulation in Golden Bay and a mean eastward drift across the northern boundary of the bays, although EFDC predicted this to be strong. Both models also predicted that the residual outflow from the bays occurs along the western side of D'Urville Island. The major difference between the two predictions occurred along the western side of Tasman Bay where the Heath (1976) prediction suggested a mean southward flow, and the present model predicted a mean northward flow. However, our model predictions are consistent with the observations of MacKenzie (2004) that the Motueka plume generally propagates northward along this coast, and that the mean flow is actually to the north.

The current meter data was used to validate the residual flows. At the eastern Tasman Bay site, the observed current residual velocity was 2.13 cm s^{-1} at 112°, whereas the predicted mean residual current velocity was considerably stronger at 8.07 cm s^{-1} although the direction was very similar at 88°. The agreement between the observed and predicted current speeds at the western side was better with the observed mean speed being 2.35 cm s^{-1}, and the predicted being 3.60 cm s^{-1}. The model predicted a mean direction of 337° by comparison with the observed mean direction of 57°. For the Golden Bay site, the observed lowpass filtered residual current velocity was 0.54 cm s^{-1} at 257° and similarly, the predicted residual velocity was 1.57 cm s^{-1} at 199°. Assuming that the observed residuals are good estimates of the long-term tidal residual flows, then the model overestimated the residual flow across the northern boundary (possibly an artefact of the boundary) and predicted a more northerly mean flow along the western side of Tasman Bay. However, because the general aspects of the residual circulation between the observations, Heath (1976) estimate, Bowman et al. (1980) estimate, and EFDC are consistent, we consider that we are reasonably close to understanding these flows. The area where the predictions diverge the most is along the western side of Tasman Bay and circulation in this region may oscillate. In other words, at times the residual flow may be southwards, somewhere in the middle of Tasman Bay (as suggested in Fig. 5), whereas at other times it may be closer to the western side, as suggested by Heath (1976).

Motueka River plume

The variation in daily mean discharge from the Motueka River during the period of the observations in 2001 demonstrated the consequences of an

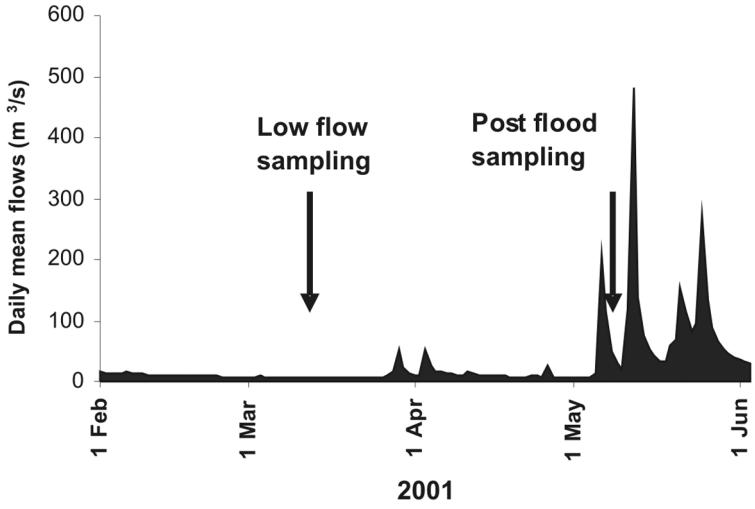

Fig. 6 Motueka River flows at Woodstock, February–May 2001. Data provided by Martin Doyle, Tasman District Council, Richmond.

Fig. 7 (*below*) Surface salinity (psu) of Motueka River plume after: **A**, low flow survey (7–8 March 2001); and **B**, post flood survey (9–10 March 2001). Data provided by L. MacKenzie, Cawthron Institute, Nelson. Grey boxes show location of proposed Aquaculture Management Areas.

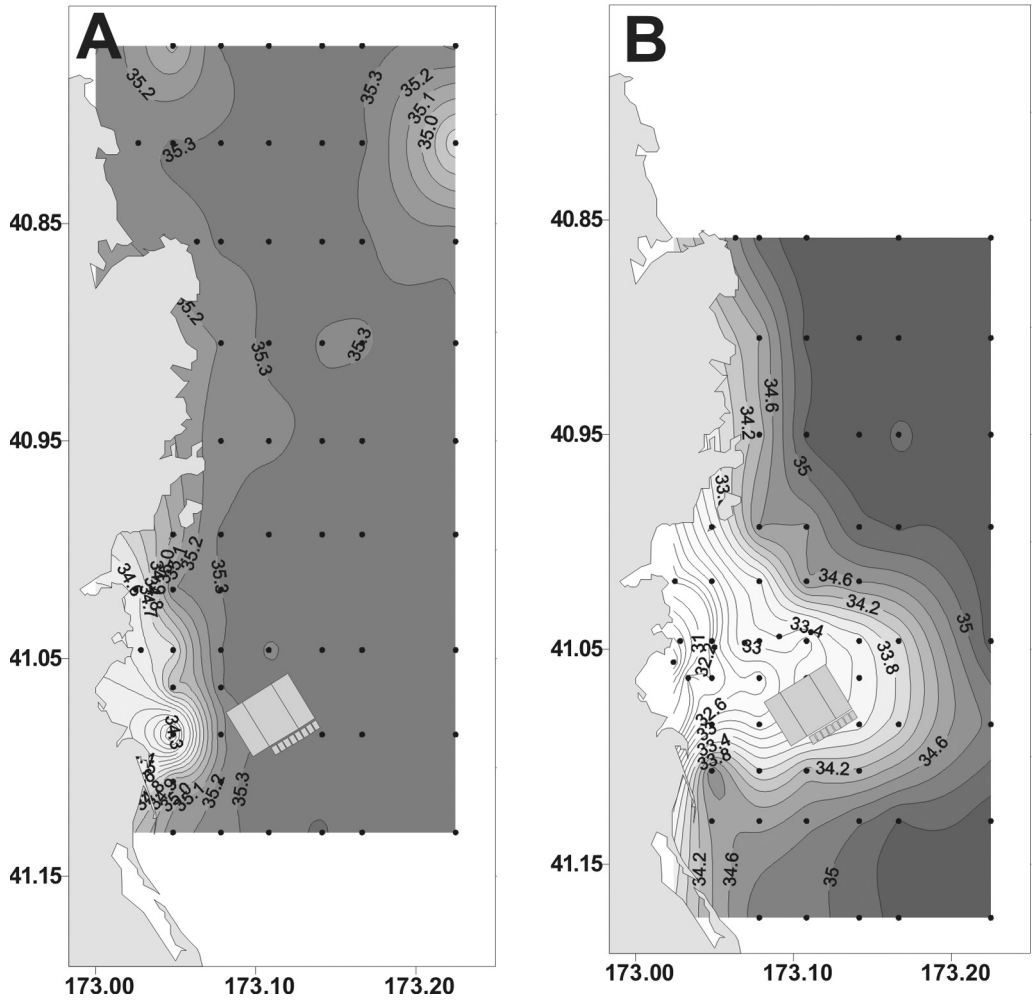

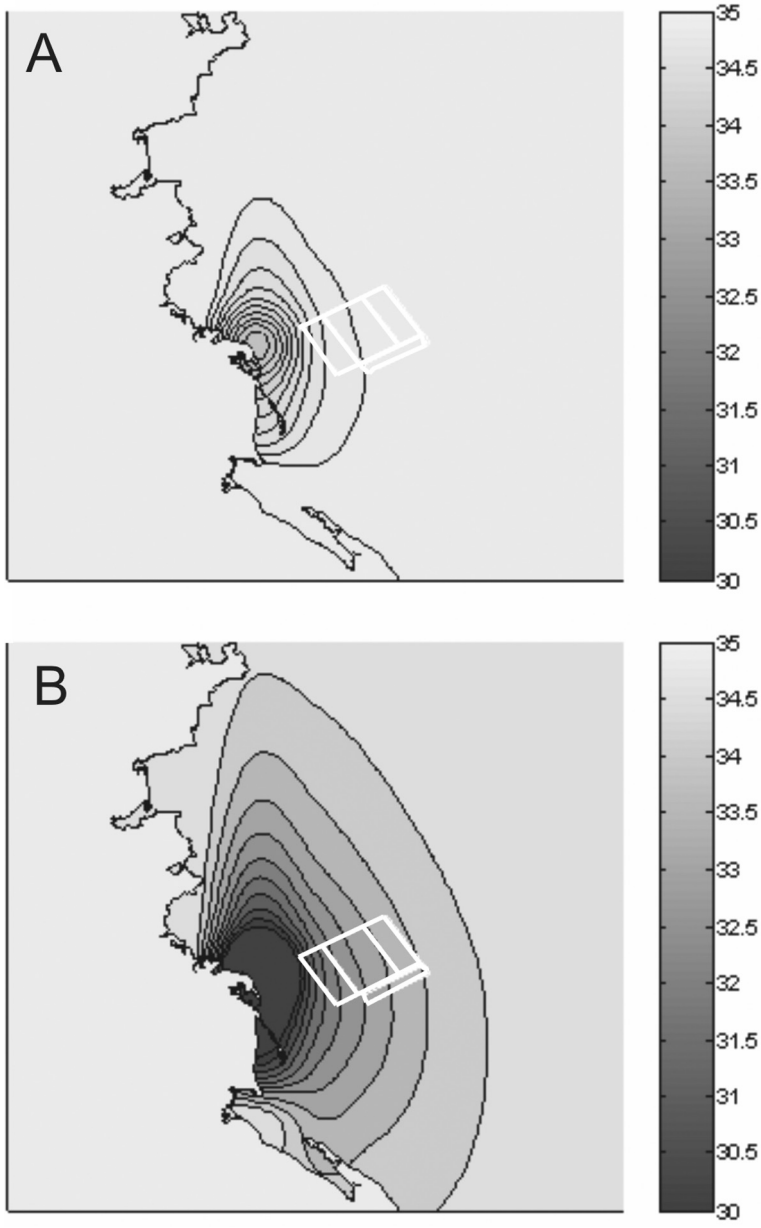

Fig. 8 Surface salinity (psu) of Motueka River plume after: **A**, low flow (10 $m^3 s^{-1}$) simulation; and **B**, flood flow (200 $m^3 s^{-1}$) simulation. White boxes show location of proposed Aquaculture Management Areas.

extended period of low flow during February and March followed by a series of rainfall events during May (Fig. 6). Direct observations during the two contrasting periods showed large differences between the pre-flood and immediate post-flood surface salinity fields (Fig. 7). Comparison of these observations with a simulation of the two events (Fig. 8) demonstrates that the model was successful at reproducing the gross features of the observed plume distribution. In particular, during the low flow scenario the observed salinities ranged from 34 to 35 psu, compared with 33.5 to 35 psu from the simulation. For the high flow scenario the observed salinities ranged from 30 to 35 psu, compared with 29.5 to 35 psu from the simulation. Both the observations and simulations revealed that the plume can extend considerable distances into Tasman Bay. Other simulations revealed that the plume can at

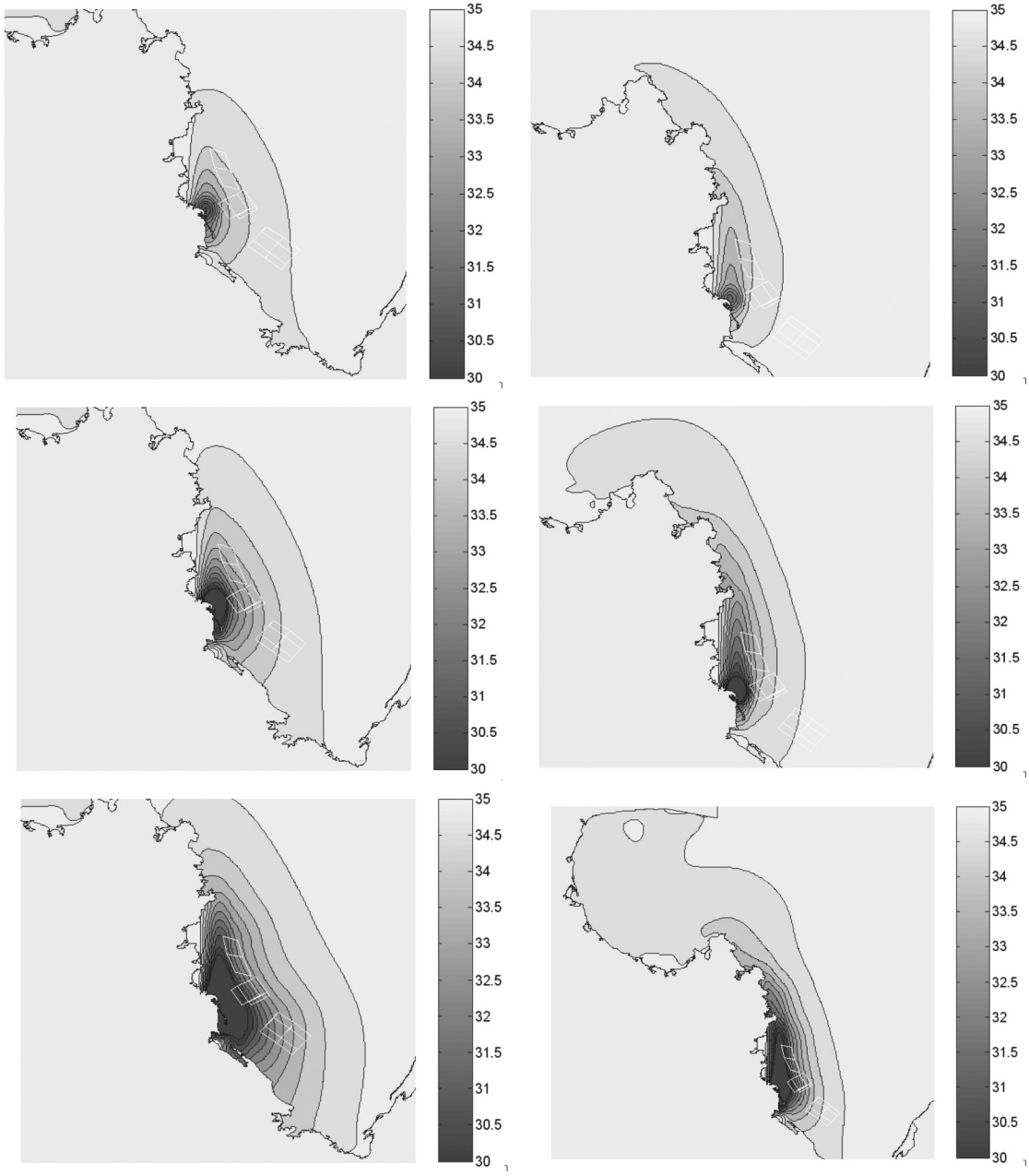

Fig. 9 Surface salinity (psu) of Motueka River plume with no wind forcing (left frames) and 20 knot southerly winds (right frames), with a flow rate of 50 $m^3 s^{-1}$ (upper frames), 200 $m^3 s^{-1}$ (middle frames), and 1000 $m^3 s^{-1}$ (lower frames). White boxes show location of proposed Aquaculture Management Areas.

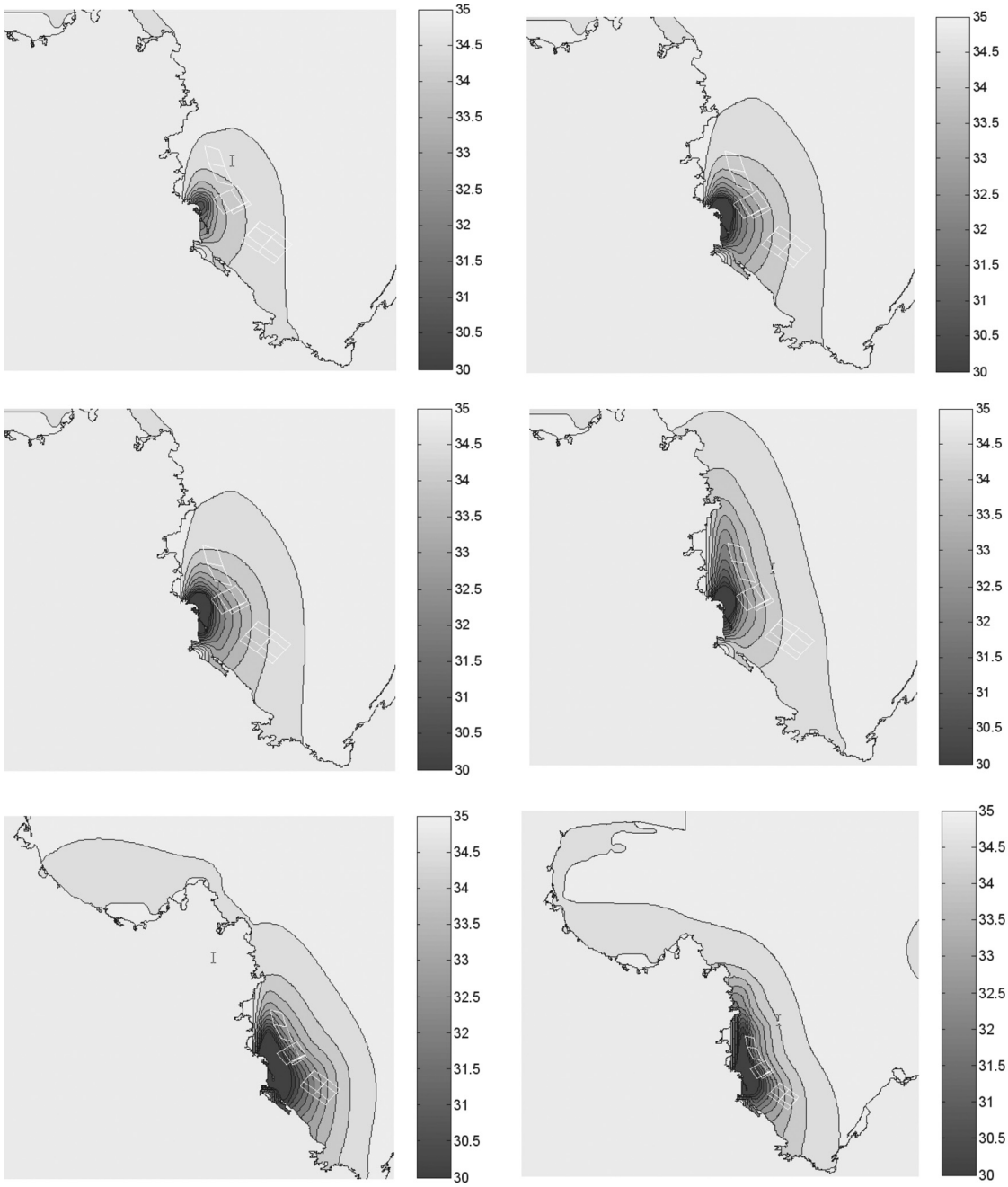

Fig. 10 Surface salinity (psu) of Motueka River plume with 20 knot north easterly winds (left frames) and 20 knot south westerly winds (right frames), with a flow rate of 50 $m^3 s^{-1}$ (upper frames), 200 $m^3 s^{-1}$ (middle frames), and 1000 $m^3 s^{-1}$ (lower frames). White boxes show location of proposed Aquaculture Management Areas.

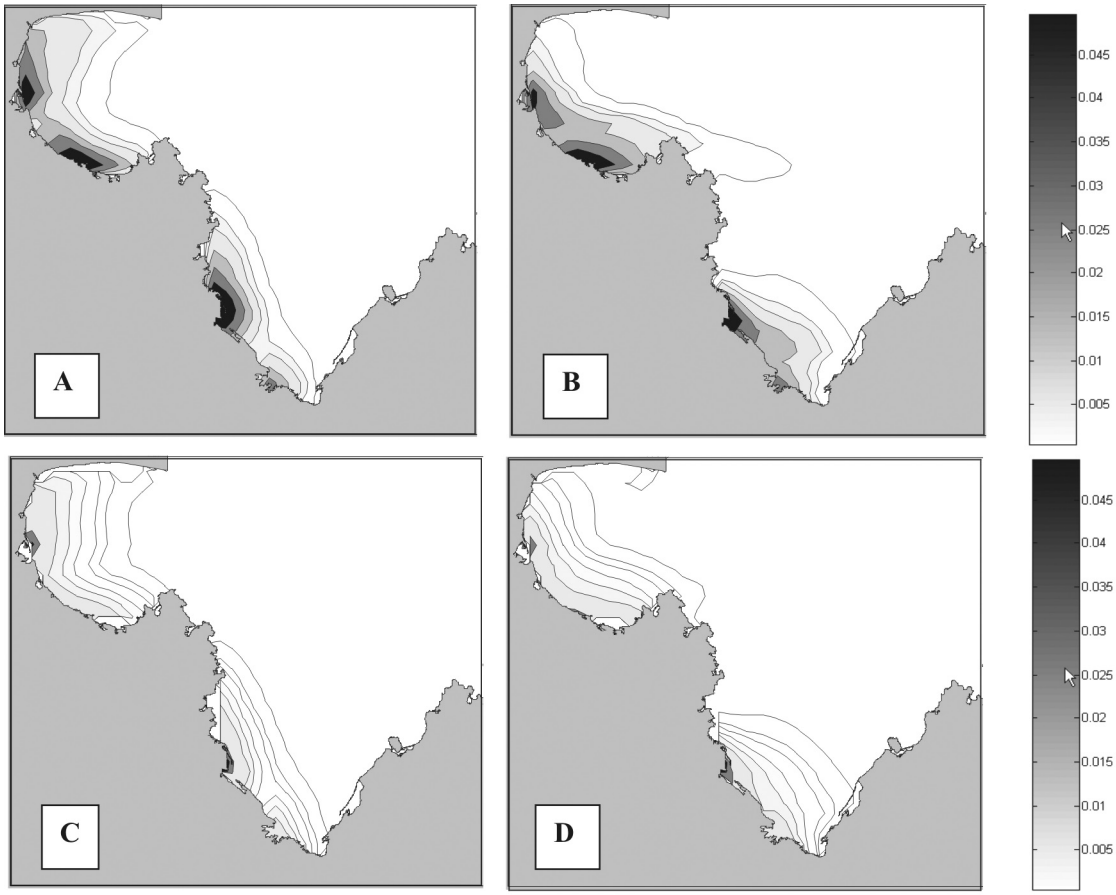

Fig. 11 **A**, **B**, Surface water concentrations (mg litre^{-1}) of suspended sediments (2 μm grain size) after 10 days baseline river flow conditions forced with no wind (left frame) and a 10 knot northerly wind (right frame). **C**, **D**, Bottom bed concentrations (g m^{-2}) of depositional sediment (2 μm grain size) after 10 days baseline river flow conditions forced with no wind (left frame) and a 10 knot northerly wind (right frame).

times extend considerable distances to the north, which is in good agreement with MacKenzie (2004) and satellite images of Tasman Bay (from Cawthron Institute AVHRR library), and that the outwelling plume can extend around Separation Point into Golden Bay (Fig. 9, 10).

Suspended sediment

Simulations of suspended and depositional sediment concentrations were affected by a variety of forcing factors. Simulations with no wind and 10 knot northerly winds are presented here for both typical baseline flows and flood events (Fig. 11–14). Since there are presently no data with which to compare the model results, the simulations are used to investigate the expected theoretical behaviour and fate of sediments introduced to the bays through river inputs. The results are presented as the surface water SS and bottom depositional sediment concentrations for each size class. Sediments with a grain size ≥20 μm did not travel far once they entered the bays (Fig. 14). It seems likely that the majority of larger sediments settle in the estuary systems that link the rivers to the coastal waters. As northerly winds typically bring rain and hence flood events to the rivers, their effects were investigated through a series of model runs using a 10 knot wind for all the sediment grain sizes. The effects of applying these northerly winds to the transport of 10 μm and 20 μm sediments was very small, but the associated

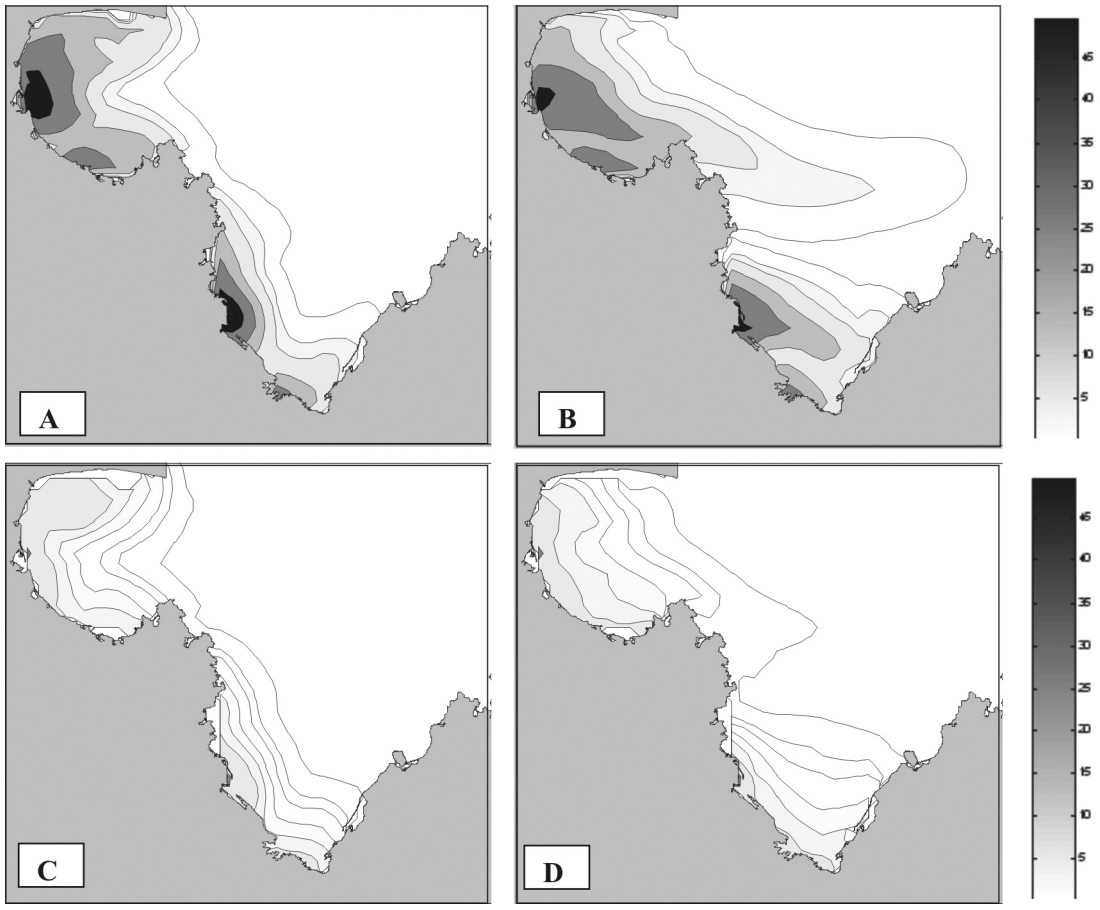

Fig. 12 **A**, **B**, Surface water concentrations (mg litre^{-1}), of suspended sediments (2 μm grain size) after 10 days flood river flow conditions forced with no wind (left frame) and a 10 knot northerly wind (right frame). **C**, **D**, Bottom bed concentrations (g m^{-2}) of depositional sediment (2 μm grain size) after 10 days flood river flow conditions forced with no wind (left frame) and a 10 knot northerly wind (right frame).

increase in the sediment load and river flows had a large effect on the transport of these sediments, as the deposition area increased markedly. However, changes in the circulation and deposition owing to the wind could be noted in the 2 μm size class (Fig. 11, 12), possibly as a result of the increased time in suspension in the water column owing to the lower sinking velocities. The change of winds associated with a passing frontal system may have an additional impact not represented by this simplified model, but it seems likely, based on these runs, that the deposition in the bays is more dependent on river flows and the associated loads than the wind. The baseline flows did not show a significant amount of sediment entering the bays for any of the size classes, even the 2 μm sediments (Fig. 11) confirming that a vast majority of the suspended sediment input is storm-related.

Investigators have often noted the presence of a near-bottom turbidity layer that appears to be a characteristic feature in Tasman Bay (Gibbs 2001; MacKenzie & Adamson 2004; Gillespie unpubl. data). A model-derived vertical profile of the normalised sediment concentration, for a site in Tasman Bay offshore of the Motueka River mouth, was compared with the direct observations of Gibbs (2001) in Fig. 15. It is of interest that the model accurately reproduced the gross trends of this feature. However, more investigation into the structure and functioning of this layer is required

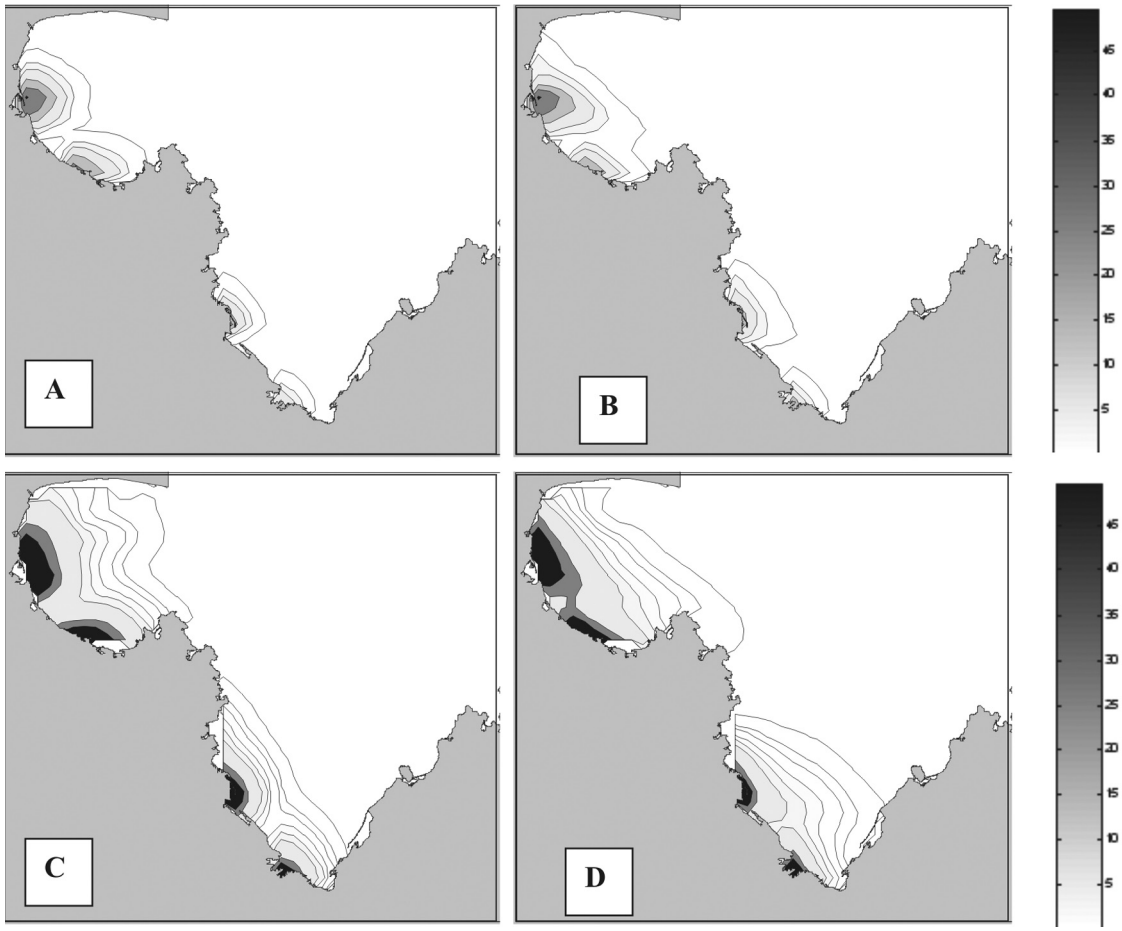

Fig. 13 **A**, **B**, Surface water concentrations (mg litre^{-1}) of suspended sediments (10 μm grain size) after 10 days flood river flow conditions forced with no wind (left frame) and a 10 knot northerly wind (right frame). **C**, **D**, Bottom bed concentrations (g m^{-2}) of depositional sediment (10 μm grain size) after 10 days flood river flow conditions forced with no wind (left frame) and a 10 knot northerly wind (right frame).

before accurate simulations of both the cohesive and non-cohesive components can be made.

Sediment input from the four major rivers included in the sediment transport model are likely responsible for the generally muddy sea floor within Tasman and Golden Bays. The particularly high flow rates of the Aorere River and to a lesser extent the Takaka River during flood events may also help to explain the shallower (largely <30 m) bathymetry of Golden Bay, as the residual currents for the area are small (<5 cm s^{-1}) and a considerable amount of the sediment (10+ μm grain size) is likely to settle within the confines of the bay. Riverine influences extend to the 2 μm sediments, where depositional sediments can be seen to accumulate in the northwestern corner of Golden Bay, at the southwestern end of Farewell Spit.

CONCLUSIONS

Despite the complexity of the tidal forcing in the region, the model was able to reproduce the gross features of the major tidal flows within the system. The general aspects of the predicted tidal circulation were in good agreement with previous limited investigations although this study suggests that the residual currents on the western side of Tasman Bay may be directed to the north, as seen in Fig. 16, in contrast to previous studies. As previously suggested, the model indicates that the D'Urville Current divides into two branches off Separation Point. One branch flows clockwise around Golden Bay but instead of the other branch flowing counter-clockwise around Tasman Bay, it flows through the

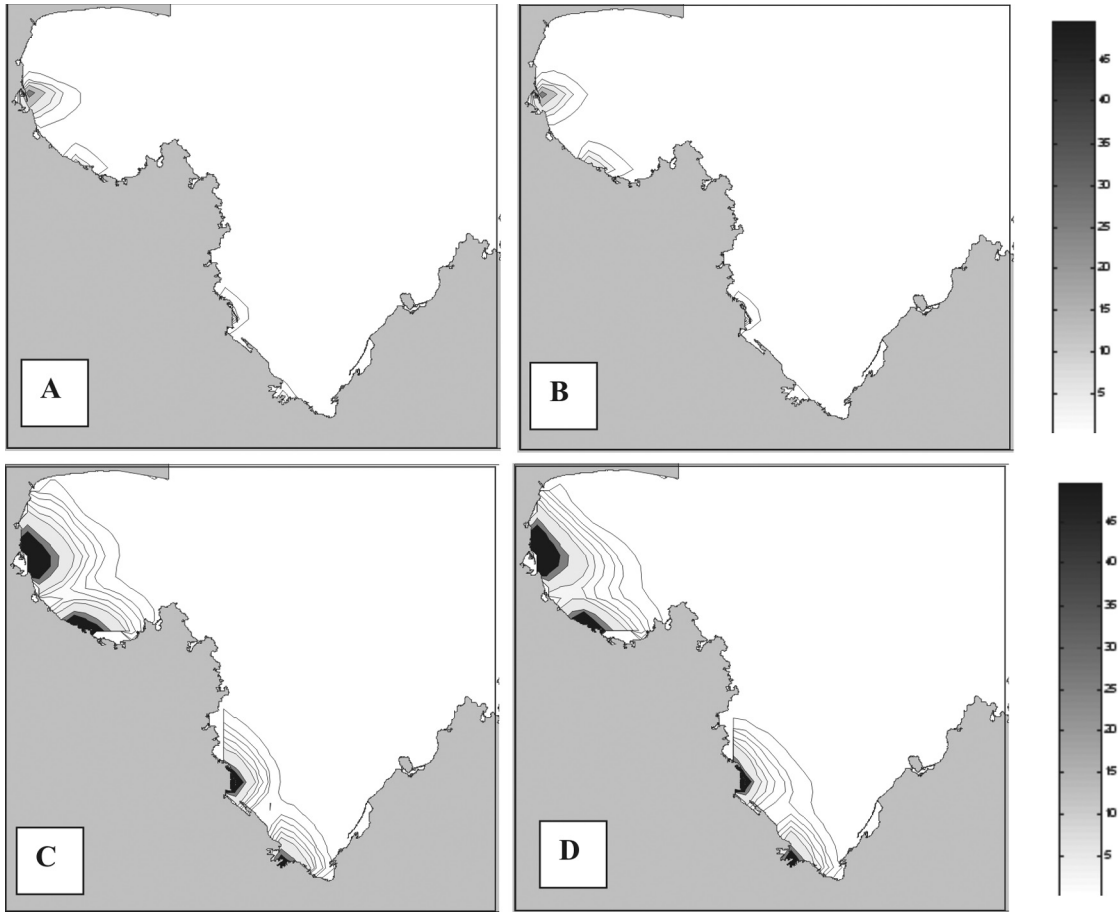

Fig. 14 **A**, **B**, Surface water concentrations (mg litre^{-1}) of suspended sediments (20 μm grain size) after 10 days flood river flow conditions forced with no wind (left frame) and a 10 knot northerly wind (right frame). **C**, **D**, Bottom bed concentrations (g m^{-2}) of depositional sediment (20 μm grain size) after 10 days flood river flow conditions forced with no wind (left frame) and a 10 knot northerly wind (right frame).

middle of Tasman Bay until it reaches the shallow bathymetry at the southern end of the bay above Nelson where it divides into two additional branches. One branch flows clockwise around Tasman Bay past Motueka and around Separation Point to join up with the original clockwise flow around Golden Bay. The other branch flows counter-clockwise around Tasman Bay past Croisilles Harbour. This circulation pattern is in good agreement with existing data describing the fate of the plume from the Motueka River. It is also possible that the spatial pattern of the flows, particularly in Tasman Bay, change in accordance to local and remote winds and this will only be able to be fully quantified by an additional, more intensive oceanographic observational study.

A numerical investigation of the fate of fresh water discharged from the Motueka River, involving a number of simulations of mean and flood flows under different wind conditions, suggests that the plume represented by the salinity field can extend considerable distances into western Tasman Bay and, under large flood conditions, extend into Golden Bay. These predictions also suggest that at times the proposed Aquaculture Management Areas in the bays will be influenced by river plumes.

The predicted fate of fine sediments entering the Nelson Bays from both the Motueka and other major rivers is consistent with our general knowledge of their bathymetric and seabed characteristics. For example, the model predicts a build up of sediment

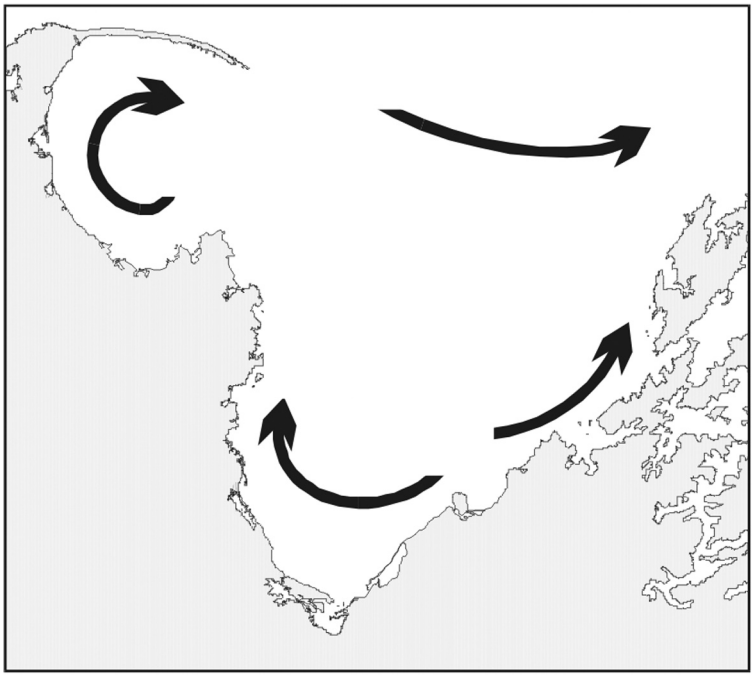

Fig. 16 Schematic tidal residual circulation for Tasman Bay/Golden Bay, New Zealand.

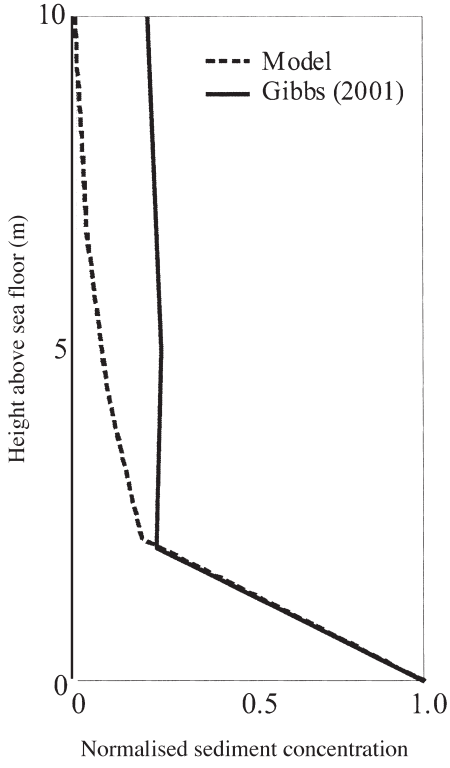

Fig. 15 Depth profile of normalised sediment concentration from model and Gibbs (2001).

inside along the southern side of Farewell Spit and this result also agrees with local knowledge of the area (Battley et al. 2005), as very fine, muddy sediments are known to make up large tidal mudflats in this corner of Golden Bay. It must be noted, however, that the modelling performed here did not include waves and wave-driven near-shore littoral drift that is likely to alter the near-shore distributions of sediments.

ACKNOWLEDGMENTS

We thank Lincoln MacKenzie for providing helpful comments on physical aspects of Tasman Bay and for unpublished surface salinity data used for model validation. Martin Doyle, Tasman District Council, also provided flow data for the major river discharges to the Nelson Bays and is thanked for his contribution. The draft manuscript was reviewed by Barry Robertson. Kim Clark assisted with the preparation of figures. This work was made possible by funding provided under Foundation for Research, Science and Technology Contract No. C09X0014.

REFERENCES

Baker AN 1972. Reproduction, early life history and age-growth relationships of the New Zealand pilchard *Sardinops neopilchardus* (Steindachner). New Zealand. Marine Department Fisheries Research Bulletin 5. 66 p.

Basher LR, Hicks DH 2003. Review of existing data on erosion rates and sediment yield for the Motueka catchment. Landcare Research Ltd, National Institute of Water and Atmospheric Research Ltd. Progress report prepared for the Integrated Catchment Management Programme. 34 p.

Battley PF, Melville DS, Schuckard R, Balance PF 2005. Quantitative survey of the intertidal benthos of Farewell Spit, Golden Bay. Marine Biodiversity Report No. 7. New Zealand Ministry of Fisheries. 48 p.

Blumberg AF, Mellor GL 1987. A description of a three-dimensional coastal ocean circulation model. In: Neaps N ed. Three dimensional Coastal Ocean Models. Vol 4. Washington DC, American Geophysical Union. 208 p.

Bowman MJ, Kibblewhite AC, Ash DE 1980. M_2 tidal effects in Greater Cook Strait, New Zealand. Journal of Geophysical Research 85: 2728–2742.

Bye JAT, Heath RA 1975. The New Zealand semi-diurnal tide. Journal of Marine Research 33: 423–442.

Carlow P, Petts G 1992. The Rivers Handbook, Vol. 1. Oxford, Blackwell Scientific Publications. 526 p.

Foreman MGG 1977. Manual for tidal heights analysis and prediction. Pacific Marine Science Report 77–10. Institute of Ocean Sciences, Patricia Bay, Victoria, British Columbia, Canada. 101 p.

Gibbs MM 2001. Sedimentation, suspension and resuspension in Tasman Bay and Beatrix Bay, New Zealand, two contrasting coastal environments which thermally stratify in summer. New Zealand Journal of Marine and Freshwater Research 35: 951–970.

Gibbs MT, Middleton JH, Marchesiello P 1998. Baroclinic response of Sydney shelf waters to local wind and deep-ocean forcing. Journal of Physical Oceanography 28: 178–190.

Gillespie PA, Maxwell PD, Rhodes LL 2000. Microphytobenthic communities of subtidal locations in New Zealand: taxonomy, biomass and food web implications. New Zealand Journal of Marine and Freshwater Research 34: 41–53.

Goring DG, Walters RA 2002. Ocean-tide loading and Earth tides around New Zealand. New Zealand Journal of Marine and Freshwater Research 36: 299–309.

Hamrick JM 1992. A three-dimensional environmental fluid dynamics computer code: theoretical and computational aspects. Special report 317. The College of William and Mary, Virginia Institute of Marine Science, United States. 63 p.

Hamrick JM 2001. EFDC1D, A one-dimensional hydrodynamic and sediment transport model for river and stream networks: model theory and users guide. Tetra Tech Inc., Fairfax, United States. 94 p.

Harris TFW 1990. Greater Cook Strait, form and flow. Wellington, DSIR Marine and Freshwater. 212 p.

Heath RA 1969. Drift card observations of currents in the central New Zealand region. New Zealand Journal of Marine and Freshwater Research 3: 3–12.

Heath RA 1976. Circulation in Tasman Bay. New Zealand Journal of Marine and Freshwater Research 10: 469–483.

Heath RA 1977. Phase distribution tidal constituents around New Zealand. New Zealand Journal of Marine and Freshwater Research 11: 383–392

LINZ 2001. New Zealand nautical almanac 2002. Auckland, Land Information New Zealand. 198 p.

Madala RV, Piaseck SA 1977. A semi-implicit numerical model for baroclinic oceans. Journal of Computational Physics 23: 167–178.

MacKenzie L 2004. River inputs, re-mineralisation and the spatial and temporal distribution of inorganic nutrients in Tasman Bay, New Zealand. New Zealand Journal of Marine and Freshwater Research 38: 681–704.

MacKenzie L, Adamson J 2004. Water column stratification and spatial and temporal distribution of phytoplankton biomass in Tasman Bay, New Zealand: implications for aquaculture. New Zealand Journal of Marine and Freshwater Research 38: 705–728.

Marchesiello P, Middleton JH 2000. Modelling the East Australian Current in the Western Tasman Sea. Journal of Physical Oceanography 30: 2956–2971.

Mellor GL 1998. Users guide for a three-dimensional, primitive equation, numerical ocean model. Program in Atmosphere and Oceanic Sciences. Princeton University. 43 p.

Proctor R, Hadfield M 1998. Numerical investigation into the effect of freshwater inputs on the circulation in Pelorus Sound, New Zealand. New Zealand Journal of Marine and Freshwater Research 32: 467–482.

Nottage RAC 2001. Water Quality of the Aorere River and its tributaries, Golden Bay. Unpublished MSc thesis, University of Otago, Dunedin, New Zealand. 133 p.

Simons TJ 1974. Verification of numerical models of Lake Ontario. Part I. Circulation in spring and early summer. Journal of Physical Oceanography 4: 507–523.

Stanton BR, Goring DG, Bell RG 2001. Observed and modelled tidal currents in the New Zealand region. New Zealand Journal of Marine and Freshwater Research 35: 397–415.

Walters RA, Goring DG, Bell RG 2001. Ocean tides around New Zealand. New Zealand Journal of Marine and Freshwater Research 35: 567–579.

Van Der Linden WJM 1969. Off-shore sediments, north-west Nelson, South Island, New Zealand. New Zealand Journal of Geology and Geophysics 12: 87–103.